Pressure-induced creation and annihilation of Weyl points in T_d-$Mo_{0.5}W_{0.5}Te_2$ and $1T''$-$Mo_{0.5}W_{0.5}Te_2$

Bishnu Karki,[1,*] Bishnu Prasad Belbase,[1,*] Gang Bahadur Acharya,[1,2] Sobhit Singh,[3,†] and Madhav Prasad Ghimire[1,2,‡]

[1]*Central Department of Physics, Tribhuvan University, Kirtipur, 44613 Kathmandu, Nepal*

[2]*Institute for Theoretical Solid State Physics, IFW Dresden, Helmholtzstrasse 20, 01069 Dresden, Germany*

[3]*Department of Physics and Astronomy, Rutgers University, Piscataway, New Jersey 08854, USA*

(Received 17 September 2021; revised 20 January 2022; accepted 10 March 2022; published 29 March 2022)

By means of first-principles density-functional theory calculations, we investigate the role of hydrostatic pressure in the electronic structure of the T_d ($Pmn2_1$) and $1T''$ (Pm) phases of the Weyl semimetal $Mo_{0.5}W_{0.5}Te_2$, which is a promising material for phase-change memory technology and superconductivity. We particularly focus on changes occurring in the distribution of the gapless Weyl points (WPs) within the 0 to 45 GPa pressure range. We further investigate the structural phase transition and lattice dynamics of the T_d and $1T''$ phases within the aforementioned pressure range. Our calculations suggest that both the T_d and $1T''$ phases of $Mo_{0.5}W_{0.5}Te_2$ host four WPs in their full Brillouin zone at zero pressure. The total number of WPs increases to 44 (36) with increasing pressure via pair creation up to 20 (15) GPa for the T_d ($1T''$) phase, and beyond this pressure pair annihilation of WPs starts occurring, leaving only 16 WPs at 45 GPa in both phases. The enthalpy versus pressure data reveal that the $1T''$ phase is more favorable below the critical pressure of 7.5 GPa; however, beyond this critical pressure the T_d phase becomes enthalpically favorable. We also provide the calculated x-ray diffraction spectra along with the calculated Raman- and infrared-active phonon frequencies to facilitate the experimental identification of the studied phases.

DOI: 10.1103/PhysRevB.105.125138

I. INTRODUCTION

The study of topological materials is of high interest at present due to their potential applications in emerging technology [1–9]. Weyl semimetals (WSMs), one class of topological materials, have attracted special attention since their experimental realization in 2015 [10–15]. Breaking of either time-reversal symmetry or spatial-inversion symmetry or both in WSMs results in a particular electronic band structure possessing crossings of the nondegenerate valance and conduction bands near the Fermi level E_F, forming gapless Weyl points (WPs) and Weyl cones [16]. The low-energy electronic excitations near these WPs behave as massless Weyl fermions [17–25]. WSMs are interesting due to their exotic properties such as WPs acting as the sources and sinks of the Berry curvature in momentum space, the existence of open Fermi-arc states connecting two opposite WPs, extremely large magnetoresistance [26–29], and various quantum Hall phenomena [30–37]. Moreover, based on the tilting of the band crossings near the Fermi level E_F, two types of WSMs are reported: (i) type-I WSMs that preserve the Lorentz invariance whose Fermi surface shrinks to zero when E_F is set at the energy of the WPs and (ii) type-II WSMs that violate the Lorentz invariance due to peculiar tilting of the Weyl cone such that WPs occur at the touching points of electron and hole pockets and whose Fermi surface never shrinks to absolute zero when E_F is set at the energy of the WPs [3,20,22,34,38,39].

WSMs belonging to the transition metal dichalcogenide (TMD) family are special, mainly because the s, p, and d orbitals in these systems hybridize to form bands near the Fermi level, which often yield various fascinating properties such as distinct quantum phase transitions between different structures, thermal and optical properties, topological domain walls, different kinds of Hall effects, and superconductivity [40–46]. Notably, dome-shaped superconducting behavior is observed in $MoTe_2$ with a transition temperature of 0.01 K that increase to 8.2 K at 11.7 GPa pressure [42,44,47–49]. $MoTe_2$ and WTe_2 are among the first reported WSMs with four WPs in their momentum space due to the broken inversion symmetry [22,50–61]. The application of external pressure and strain has been reported to play a vital role in tuning the WSM phase in $MoTe_2$ and WTe_2 [58,62–64].

Substitution of W by Mo in WTe_2, forming the polymorphic structure $Mo_xW_{1-x}Te_2$, is reported to control the structural phase transition, transport properties, thermal conductivity, Weyl phase, and superconductivity in this system [65–72]. Depending on the magnitude of the pressure applied to $Mo_xW_{1-x}Te_2$ ($x = 0.9$, 0.6, and 0.25), the superconducting transition temperature can be tuned [73]. Moreover, a tunable WSM phase and Fermi-arc states can be realized in $Mo_xW_{1-x}Te_2$ ($x \leqslant 0.5$) by varying x [74–76]. By means of the temperature-dependent elastic neutron scattering measurements, Schneeloch *et al.* [70] recently investigated the monoclinic $1T'$ to orthorhombic T_d structural phase

*These authors contributed equally to this work.
†sobhit.singh@rutgers.edu
‡madhav.ghimire@cdp.tu.edu.np

transition in $Mo_{1-x}W_xTe_2$ as a function of the W substitution and temperature. They observed that the $1T'$-T_d phase transition is accompanied by an intermediate pseudo-orthorhombic phase T_d^*, which was first reported by Tao *et al.* [72] for pure $MoTe_2$. Notably, the intermediate T_d^* phase exists only up to concentration $x = 0.34$ and vanishes for $x > 0.34$. Their results further suggest that at room temperature the $Mo_{0.5}W_{0.5}Te_2$ composition favors the T_d phase [70]. Marchenkov *et al.* [71] experimentally studied the transport and optical properties of single-crystal $Mo_{0.5}W_{0.5}Te_2$. Their temperature-dependent resistivity data revealed the metallic nature of the system. Li *et al.* recently performed dimensionality-dependent transport measurements on a special $Mo_{0.5}W_{0.5}Te_2$ sample having a thickness gradient across two- and three-dimensional regimes and reported strong evidence that this material is a type-II WSM [77].

The experimental observation of pressure-controlled superconductivity in $Mo_{0.5}W_{0.5}Te_2$ [73] calls for a systematic investigation of the pressure-induced changes occurring in the crystal structure, electronic structure, and WSM phase of this system. In this work, we theoretically study the structural, vibrational, and topological electronic properties of $Mo_{0.5}W_{0.5}Te_2$ as a function of the hydrostatic pressure within a 0 to 45 GPa pressure range. We explore the aforementioned properties of two candidate crystal phases of $Mo_{0.5}W_{0.5}Te_2$, T_d and $1T''$, as a function of the applied pressure. Our calculations indicate that both of these phases are dynamically stable within the studied pressure range and both of them host a number of WPs in their momentum-energy space. Interestingly, WPs in both phases can be created via pair creation, destroyed via pair annihilation, and shifted in the momentum-energy space by application of external pressure. Such tunability of the Weyl phase is desired to harness various transport and optical properties of WSMs [2–4,78–81], particularly those associated with the nonzero Berry-curvature dipole such as the nonlinear Hall effect [82,83], circular photogalvanic effect [84–86], and nonlinear optical responses [86–88]. Furthermore, creation (annihilation) of WPs near the Fermi level as well as their shifting in the momentum-energy space can enhance (suppress) electronic transport properties in WSMs. Our work implies that $Mo_{0.5}W_{0.5}Te_2$ exhibits a variety of interesting topological properties at higher pressures, and it may provide a novel platform for the realization of Weyltronics. Furthermore, our results suggest an increase in the superconducting transition temperature at higher pressures, which is in agreement with recent experimental observations [43,73].

II. COMPUTATIONAL DETAILS

The density-functional theory (DFT) calculations were performed using the projector augmented wave (PAW) method as implemented in the Vienna Ab initio Simulation Package (VASP) [89–91]. Six valence electrons were considered in the PAW pseudopotentials of Mo, W, and Te. The Perdew-Burke-Ernzerhof generalized gradient approximation (GGA) was used to compute the exchange-correlation functional [92]. The GGA-opt86b is more accurate exchange functional used for the van der Waals (vdW) density-functional corrections [93–95]. The reciprocal space was sampled using a Γ-centered k mesh with a size of $8 \times 12 \times 4$ together with a kinetic energy cutoff of 600 eV for plane waves. The energy and force convergence criteria were set to 10^{-8} eV and 10^{-4} eV/Å, respectively. The hydrostatic pressure was applied up to 45 GPa. The crystal structures were fully optimized in the inner coordinates as well in the cell parameters for each pressure considering spin-orbit coupling (SOC) and GGA-opt86b vdW corrections [93–95]. All the DFT calculations were carried out in a 12-atom unit cell of $Mo_{0.5}W_{0.5}Te_2$. The optimized lattice parameters for the T_d phase at zero pressure are $a = 6.301$, $b = 3.490$, and $c = 14.076$ Å, and cell angles are $\alpha = \beta = \gamma = 90^\circ$, which are in excellent agreement with the experimental data reported in Ref. [70].

The phonon calculations were performed using the finite-difference approach using $2 \times 3 \times 1$ supercells. SOC was considered in all phonon calculations. The PHONOPY [96] package was utilized to plot the phonon dispersions. The MECHELASTIC [97,98] package was used to perform the equation of states (EOS) analyses using the enthalpy versus pressure data. In order to understand the distribution of Weyl points in the momentum-energy space, we compute the real-space Wannier Hamiltonian using the full potential local orbital (FPLO) code, version 18 [99]. We employed the above-mentioned DFT convergence parameter in all the FPLO calculations. The Wannier fitting was done using the PYFPLO [99] module of the FPLO package considering Mo $4d$ and $5s$, W $5d$ and $6s$, and Te $5s$ and $5p$ as the local orbital basis. The PYPROCAR code [100] was used to investigate the DFT-calculated electronic band structures, and VESTA [101] software was used to draw the crystal structures.

III. RESULTS AND DISCUSSION

A. Crystal structures

In order to theoretically investigate the electronic structure of $Mo_{0.5}W_{0.5}Te_2$, we prepare two candidate crystal structures, as shown in Figs. 1(a) and 1(b), by taking the parent T_d phase (space group $Pmn2_1$) of WTe_2 and systematically substituting one W atom by one Mo atom in each vertically stacked layer. There are two possible ways to carry out such a substitution. First, we consider a scenario in which the ordering of Mo and W atoms is reversed in the adjacent vertically stacked layers, i.e., (Mo-W)$\cdots$(W-Mo)$\cdots$(Mo-W)$\cdots$. This results in a crystal structure belonging to space group $Pmn2_1$ (No. 31), similar to the parent T_d phase; hence, we call this structure the T_d phase. Note that this structure retains the vertical glide-mirror symmetry, as discussed in Ref. [37]. Also, this structure does not break the orthorhombic symmetry of the parent T_d structure after a free DFT relaxation.

Second, we consider a scenario in which ordering of the Mo and W atoms remains the same within the adjacent vertically -stacked layers, i.e., (Mo-W)$\cdots$(Mo-W)$\cdots$(Mo-W)$\cdots$. Such a configuration breaks the vertical glide-mirror symmetry [37] and results in space group Pm (No. 6) after a free DFT relaxation of the unit cell. Note that the optimized structure is slightly distorted from the parent orthorhombic cell to a distorted monoclinic cell with a monoclinic cell angle of $\beta \neq 90^\circ$, which varies as a function of the applied hydrostatic pressure, as we discuss below. Although this monoclinic structure is similar to the $1T'$ phase (space group $P2_1/m$) of

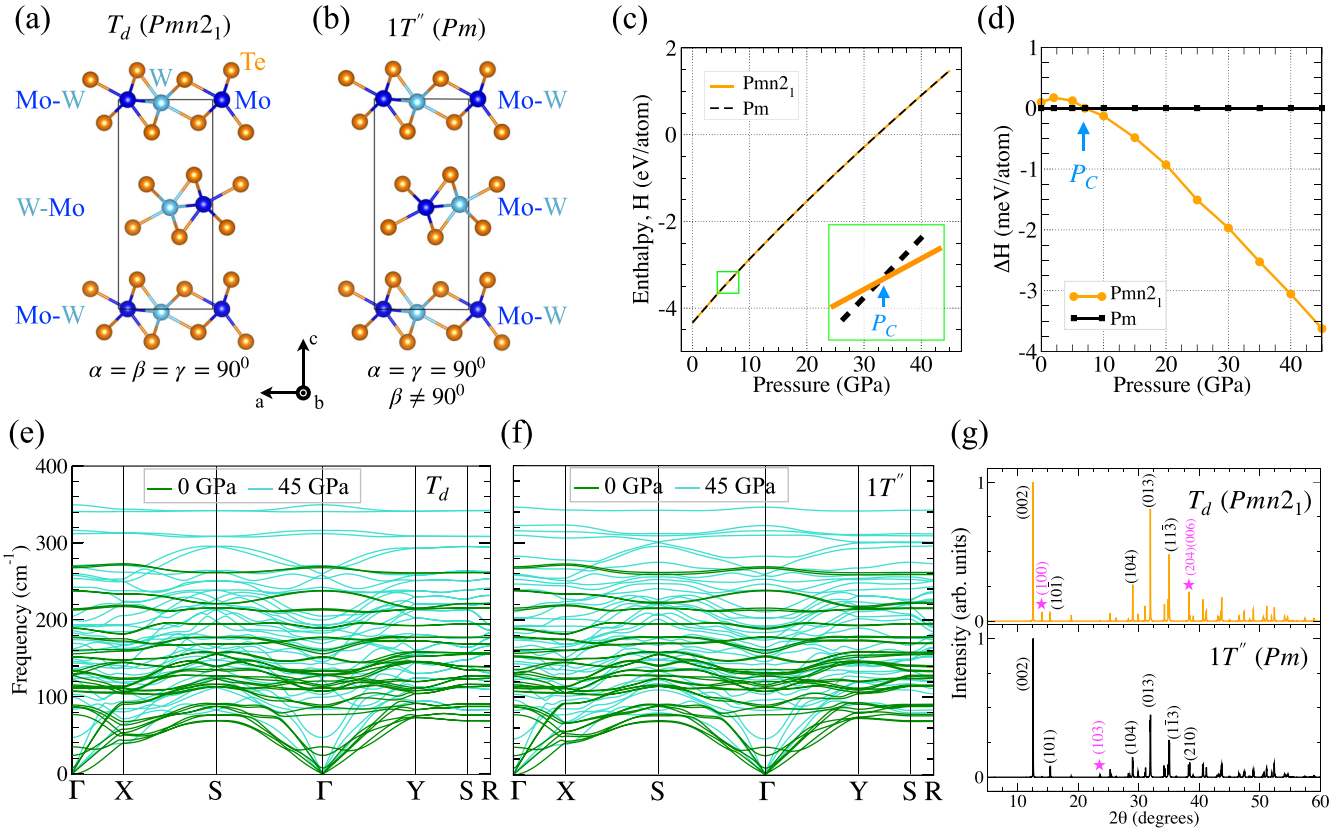

FIG. 1. (a) and (b) Crystal structures of the T_d and $1T''$ phases of $Mo_{0.5}W_{0.5}Te_2$. Note that $1T''$ has a subtle monoclinic distortion due to the cell angle $\beta \neq 90°$. (c) Enthalpy versus pressure phase diagram for the T_d and $1T''$ phases. The critical pressure P_C at which the structural phase transition occurs is predicted to be near 7.5 GPa. Inset: an enlarged view near the crossing point. (d) The enthalpy difference ΔH ($= H_{T_d} - H_{1T''}$) as a function of pressure. (e) and (f) Calculated phonon spectra (with SOC) at 0 and 45 GPa pressure for the T_d and $1T''$ phases. We would like to note that we decided to plot the phonon dispersion for the $1T''$ phase along the same high-symmetry k path as in the T_d phase for the sake of better comparison, although the $1T''$ phase has a subtle monoclinic distortion (see the SM [102] for details). (g) The calculated x-ray diffraction (XRD) patterns for the T_d and $1T''$ phases at 0 GPa pressure. The signature peaks in both phases are marked in magenta. More details about the crystal structures, calculated XRD patterns, phonon spectra calculated at higher pressures, and a comparison of the calculated Raman-active phonon frequencies with the available experimental data are provided in the SM [102].

TMDs, it is lower in symmetry due to the broken inversion and vertical glide-mirror symmetries [37]. Therefore, we decide to call this monoclinic phase the $1T''$ phase. We note both of the structures, T_d and $1T''$, have broken inversion symmetry, which is a fundamental requirement for nonmagnetic Weyl semimetals.

Before moving further, let us briefly discuss the possible reason behind the observed monoclinic distortion in the $1T''$ phase. One could imagine the presence of an in-plane polarity orientation determined by the peculiar ordering of Mo and W atoms with different electronegativities within each vertically stacked layer, as shown in Figs. 1(a) and 1(b). In Fig. 1(a), where the ordering of Mo-W pairs is reversed as we move in the vertical direction, the in-plane polarity would reverse its sign in the adjacent vertically stacked layers, i.e., $-+-+\cdots$ or $+-+-\cdots$ (antipolar order). Here, $+$ and $-$ signs denote the polarity orientation parallel or antiparallel to the a lattice vector. In such a configuration, a free relaxation of structure does not require any monoclinic distortion of the orthorhombic cell due to the perfect cancellation of dipolarlike interactions along the vertical direction (not strictly speaking because partial screening of electric dipoles may occur due to the semimetallic nature of this system). On the other hand, in Fig. 1(b), where the ordering of Mo-W pairs is the same in the adjacent vertical layers, the in-plane polarity would be parallel in the adjacent layers, i.e., $----\cdots$ or $++++\cdots$, similar to that of the $1T'$ phase [37,46]. Hence, in order to minimize the total free energy such structures tend to exhibit a monoclinic distortion due to the sliding of the adjacent polar layers along the in-plane direction, as discussed in Ref. [37].

B. Pressure-induced effects on the T_d and $1T''$ structures

Next, we test the relative stability of the T_d and $1T''$ phases as a function of pressure. Our calculations reveal that the enthalpy difference ΔH between these two phases is very small [Figs. 1(c) and 1(d)]. This implies the likelihood of the formation of a solid solution of the T_d and $1T''$ phases at finite temperatures. We find that below the critical pressure ($P_C =$ 7.5 GPa), the $1T''$ phase is more favorable, whereas above P_C the T_d phase is preferred. We further performed the EOS analyses using the Birch, Vinet, and Birch-Murnaghan models as implemented in the MECHELASTIC package [97,103,104].

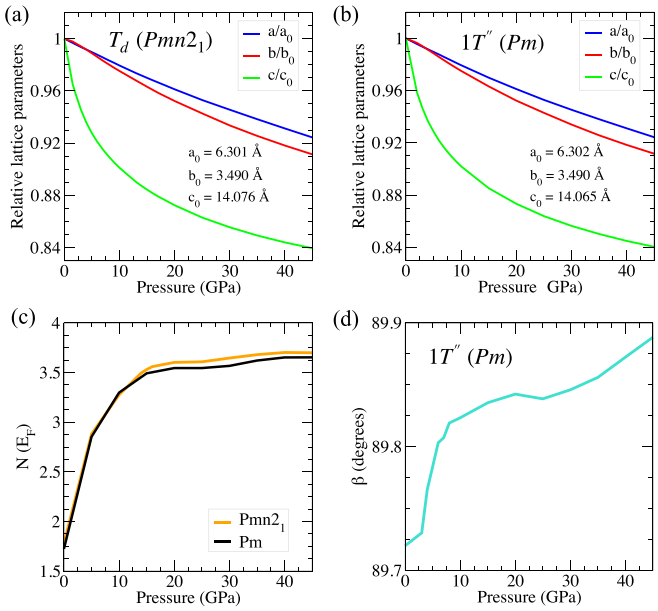

FIG. 2. (a) and (b) The optimized lattice parameters normalized to the lattice parameters obtained at zero pressure (a_0, b_0, c_0) and (c) the calculated density of states (states/eV) at the Fermi level $N(E_F)$ plotted as a function of pressure for both the T_d and $1T''$ phases. (d) Pressure-dependent variation in the monoclinic cell angle β for the $1T''$ phase. Note that $\beta = 90^\circ$ for the T_d phase.

The difference between the obtained EOS fitting parameters for the T_d and $1T''$ phases is minimal (see the Supplemental Material (SM) [102] for more details).

The phonon spectra calculated considering the SOC and vdW corrections for both the T_d [Fig. 1(e)] and $1T''$ [Fig. 1(f)] phases demonstrate the dynamical stability of these phases at zero pressure as well as at higher pressures (see the SM [102]). We notice an increase in the phonon frequencies with increasing pressure; that is, phonons harden at higher pressures. No dynamical instability was observed in either phase within the studied pressure range. A list of the infrared- and Raman-active phonon frequencies calculated at different pressures is provided in the SM [102]. We hope this can facilitate experimental identification of the T_d and $1T''$ phases.

Furthermore, we calculate the x-ray diffraction (XRD) patterns of the T_d and $1T''$ phases at various pressures using a Cu $K\alpha$ x ray with a wavelength of 1.5406 Å. Figure 1(g) shows the calculated XRD patterns at zero pressure (data at higher pressure are provided in the SM [102]). Although the calculated XRD spectra look quite similar for both phases, there are some signature peaks, marked using magenta stars, which are present in one phase but absent in the other. These peaks can be used to distinguish between the T_d and $1T''$ phases in real crystals. Notably, the calculated peak position for the (002) crystallographic peak and the Raman-active phonon frequencies (see the SM [102]) match remarkably well with the reported experimental data for $Mo_{0.5}W_{0.5}Te_2$ single crystals [65].

Figures 2(a) and 2(b) show the pressure dependence of the DFT optimized lattice parameters for the T_d and $1T''$ phases. We observe a very similar trend in the pressure-dependent structural parameters of both phases. To highlight the observed trend, we plot the normalized lattice parameters with respect to the lattice parameters obtained at zero pressure. We observe the maximum change in the c lattice parameter with varying pressure. At 45 GPa, the c lattice parameter decreases by ∼15% for both phases, whereas the relative change in the a and b lattice parameters is less than 10% within the studied pressure range. Such behavior is expected owing to the weak vdW interaction along the out-of-plane c axis. The optimized Mo-W bond length shows a pressure-dependent behavior similar to that of the in-plane lattice parameters. The Mo-W bond length decreases from a value of 2.85 Å at zero pressure to 2.70 Å at 45 GPa. This is an almost 5% decrease in the Mo-W bond length. On the other hand, the maximum compression in the Mo-Te and W-Te bond lengths is nearly 4% at 45 GPa.

Strikingly, the Te-Te interlayer distance undergoes the maximum change (∼24%) as a function of external pressure in both the T_d and $1T''$ phases; the optimized Te-Te interlayer distance decreases from 3.93 Å at zero pressure to 2.98 Å at 45 GPa. References [73,105] pointed out that such a softening of the Te-Te interlayer vibrational mode substantially contributes to the overall electron-phonon coupling, which could possibly be the origin of the emergence of superconductivity in this system.

Figure 2(d) shows the variation in the monoclinic angle β as a function of the pressure for the $1T''$ phase. With increasing pressure, the cell angle β tends to approach 90°, which implies a decrease in the monoclinic distortion and a preference for the orthorhombic T_d phase at higher pressures. This is consistent with the data shown in Fig. 1(d).

Since $Mo_{0.5}W_{0.5}Te_2$ is particularly interesting due to its superconducting properties [73], we calculate the density of states at the Fermi level $N(E_F)$ as a function of pressure for both the T_d and $1T''$ phases, as shown in Fig. 2(c). A systematic increase in $N(E_F)$ with increasing pressure was observed in both phases. We would like to note that phonons also harden with increasing pressure [see Figs. 1(e) and 1(f)]. Thus, an increased $N(E_F)$ together with the higher phonon frequencies implies an enhancement in the effective electron-phonon coupling at higher pressures, which could substantially increase the superconducting transition temperature in this system at higher pressures [47,105–107]. This is consistent with recent experimental observations [43,73].

C. Pressure-tunable Weyl semimetal phase

The band structure calculations of the T_d and $1T''$ phases for different pressures are presented in Figs. 3 and 4. The topmost valence band indicated in green forms the hole pocket, and the bottom of the conduction band indicated in red forms the electron pocket near E_F along the Γ-X, S-Γ-Y, and U-Z-T high-symmetry directions of the Brillouin zone (BZ) [108]. These electron and hole pockets touch each other at discrete points in the momentum space, forming type-II WPs [22]. The change in pressure affects the size of the electron and hole pockets in the momentum space. With increasing pressure, these pockets come close to each other, producing more band crossings, as implied in Figs. 3 and 4. A similar trend is found for the $1T''$ phase.

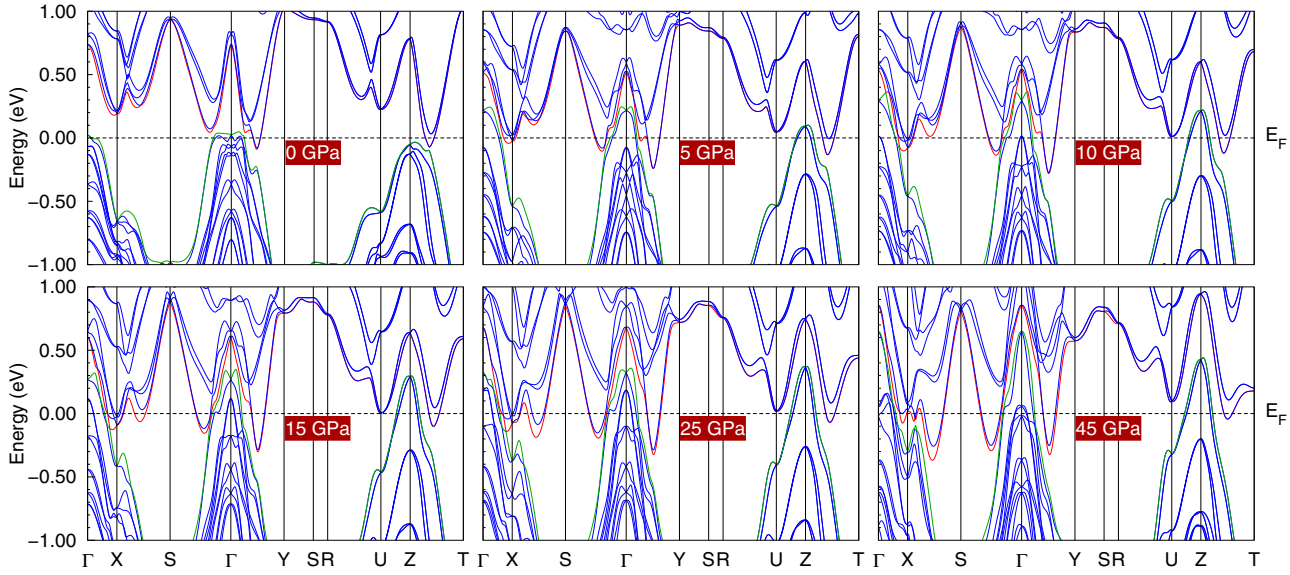

FIG. 3. Band structures of the T_d phase calculated at pressure values of 0, 5, 10, 15, 25, and 45 GPa with the inclusion of SOC. Red in the band structures represents the lowest conduction band, and green represents the highest valence band. The dashed horizontal line marks E_F ($E_F = 0$ eV).

TMDs are the first class of materials to host type-II WPs. Soluyanov *et al.* first reported type-II WPs in pure WTe_2 located between 0.052 and 0.058 eV above E_F [22]. Sixteen WPs are found in k space with eight WPs at the $k_z = 0$ plane and eight more WPs off the plane ($k_i \neq 0$, $i = x$, y, and z). With inclusion of SOC all the WPs at $k_i \neq 0$ are annihilated, leaving only 8 of the 16 WPs. Similarly, Sun *et al.* predicted the type-II WSMs in $MoTe_2$ [58]. Eight WPs are recorded at two different energies, 6 and 59 meV above E_F.

Here, in our study with 50% substitution of Mo on WTe_2 without the application of pressure, we report four WPs at an energy state 55 meV above E_F at the $k_z = 0$ plane for the T_d phase. In contrast, a similar number of WPs are recorded for the $1T''$ phase but at a different energy state, 93 meV below E_F at the $k_z \neq 0$ plane. The energy of the WPs obtained for the T_d phase is in agreement with the energy of WPs for $MoTe_2$ [58] and WTe_2 [22], whereas the $1T''$ phase hosts WPs below E_F. Moreover, the chemical effect is also found to play a significant role in the change in the total number of WPs in $Mo_{0.5}W_{0.5}Te_2$.

We obtain a total of four WPs (W_1) in the first BZ of the T_d and $1T''$ phases of $Mo_{0.5}W_{0.5}Te_2$ at zero pressure. The coordinates of the nonequivalent W_1 WPs are given in Table I; the other three WPs are the mirror reflections of W_1 at zero

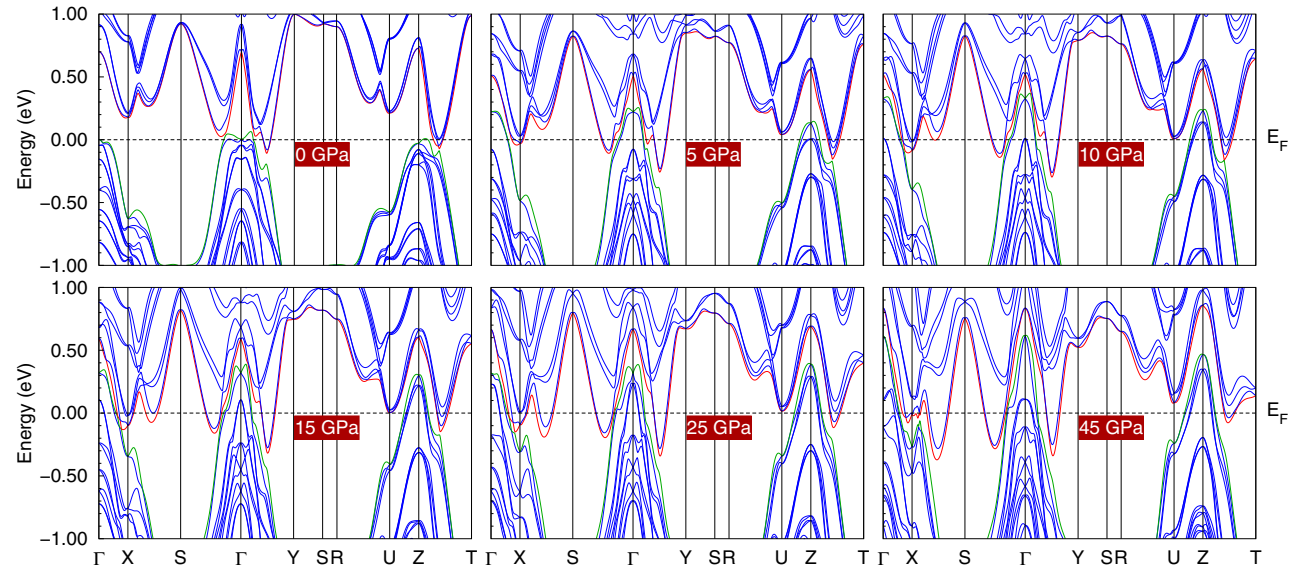

FIG. 4. Band structures of the $1T''$ phase calculated at pressure values of 0, 5, 10, 15, 25, and 45 GPa with the inclusion of SOC. Red in the band structures represents the lowest conduction band, and green represents the highest valence band. The dashed horizontal line marks E_F. For a better comparison the k paths of the $1T''$ phase are also chosen to be the same as in the T_d phase.

TABLE I. Location of W_1 WPs in the momentum space of the T_d and $1T''$ phases at zero pressure

WP	$k_x\left(\frac{2\pi}{a}\right)$	$k_y\left(\frac{2\pi}{b}\right)$	$k_z\left(\frac{2\pi}{c}\right)$	Chirality χ
$W_1(T_d)$	−0.132	−0.095	0.000	+1
$W_1(1T'')$	−0.004	−0.200	−0.416	+1

pressure. There is variation in the total number and locations of WPs due to the application of hydrostatic pressure. Below we discuss the role of the hydrostatic pressure in the Weyl phase of T_d- and $1T''$-$Mo_{0.5}W_{0.5}Te_2$.

1. Pressure effects on the T_d phase

The variation in the number of WPs and their energy states for the T_d phase is presented in the graphical plots in Figs. 5(a) and 5(b). On increasing the pressure value to 1.5 GPa new sets of WPs, W_2 and W_3, are generated along with the initial W_1, making the total number of WPs 20. Here, we notice that the pressure shifts the energy state of W_1 to $E_F + 75$ meV. The eight newly created copies of W_2 and W_3 are found in the energy states of $E_F + 8$ meV and $E_F - 7$ meV, respectively. No further creation of WPs up to a pressure of 8 GPa occurs; the position and energy states of the WPs simply vary with the pressure. The energy state of W_1 rises to the highest value of $E_F + 139$ meV at 8 GPa pressure and decreases on a further increase of the pressure, getting closest to the Fermi level (energy state $E_F + 1$ meV) at 35 GPa and shifting below the Fermi level above that pressure. The pair creation of W_4 and W_5, each with four WPs, occurs at 9 GPa and continues up to 10 GPa, getting annihilated above that pressure. The highest number of WPs is observed at 20 GPa, and a constant number of 16 WPs is observed at 30 to 45 GPa.

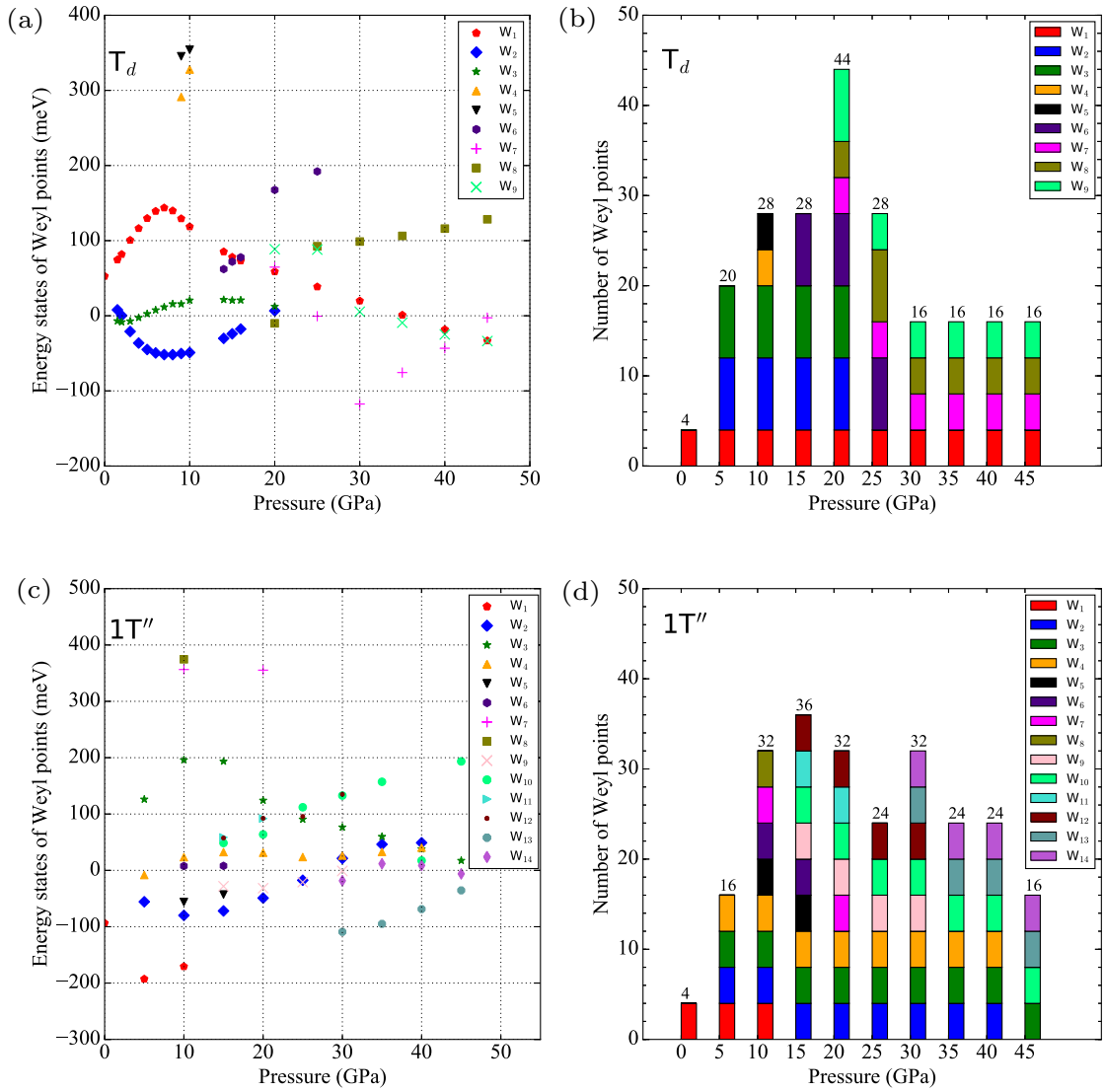

FIG. 5. (a) Energy states of WPs with respect to E_F calculated at different values of pressure for the T_d phase. (b) Stack-bar diagram showing the creation and annihilation of the WPs from 0 to 45 GPa for the T_d phase. (c) Energy states of WPs corresponding to different pressures for the $1T''$ phase. (d) Stack-bar diagram showing the creation and annihilation of the WPs from 0 to 45 GPa for the $1T''$ phase. The total number of WPs at each pressure is written at the top of each bar. See the SM [102] for more details regarding the number and location of WPs obtained at each pressure.

2. Pressure effects on the 1T″ phase

Pressure also has an impact on the dynamics of WPs in the $1T''$ phase. Pair creation and annihilation of WPs as a function of pressure are noticed in the momentum space of the $1T''$ phase. Here, the W_1 WPs continue to exist up to 10 GPa, getting annihilated with a further rise in pressure. Similarly, the W_2 WPs are created at 5 GPa pressure and exist up to 40 GPa and then get annihilated. A similar phenomenon of pair creation and annihilation is noticed for the other energy state of WPs as well, which is summarized in Figs. 5(c) and 5(d). More energy states of the WPs are observed in the $1T''$ phase compared to the T_d phase due to its lower symmetry. In terms of the total number of WPs, the highest number of 36 is observed at 15 GPa pressure, whereas a constant number of 16 WPs is noticed for pressures beyond 40 GPa.

IV. SUMMARY

In summary, we studied the structural, vibrational, electronic, and topological Weyl properties of $Mo_{0.5}W_{0.5}Te_2$ by means of first-principles DFT calculations. We found that there are two possible candidate structures, T_d and $1T''$, for 50:50 Mo:W substitution. We studied the aforementioned properties of these two phases in the 0–45 GPa pressure range. We found that both structures are energetically and dynamically stable in the studied pressure. The calculated x-ray diffraction spectra and the infrared- and Raman-active phonon frequencies indicate that these two phases can be identified in experiments, although they are likely to form solid solutions due to the subtle difference in their enthalpies at low pressures. The T_d ($1T''$) phase is theoretically more favorable at higher (lower) pressures, with the critical pressure being 7.5 GPa. Our calculations revealed that the density of states and phonon frequencies increase dramatically with increasing pressure in both phases, which is indicative of larger electron-phonon coupling at higher pressures, and it could substantially increase the superconducting transition temperature in this system at higher pressures.

Interestingly, we found that both the T_d and $1T''$ phases host a number of WPs in their momentum-energy space. The total number and location of WPs can be controlled by varying hydrostatic pressure. Four WPs were obtained in the T_d and $1T''$ phases at zero pressure. The total number of WPs increased to 44 (36) with increasing pressure, via pair creation, up to 20 (15) GPa for the T_d ($1T''$) phase, and beyond this pressure, pair annihilation of WPs started occurring, leaving only 16 WPs at 45 GPa in both phases. Therefore, we can conclude that pressure can tune WPs to the desired location, generate new WPs, and also annihilate them, thus providing an ideal platform for the realization of Weyltronics in $Mo_{0.5}W_{0.5}Te_2$.

ACKNOWLEDGMENTS

M.P.G. acknowledges the Alexander von Humboldt Foundation, Germany, for the equipment grants and IFW-Dresden for providing the large-scale computer nodes to the Advanced Materials Research Laboratory for scientific computations. S.S. acknowledges funding from Office of Naval Research (ONR) grant N00014-21-1-2107. This work was supported by the U.S. Department of Energy (DOE), Office of Science, Basic Energy Sciences under award DE-SC0020353 (S.S.). G.B.A. thanks the Nepal Academy of Science and Technology for the Ph.D. fellowship. M.P.G. and G.B.A. thank M. Richter for fruitful discussions and U. Nitzsche for technical assistance.

[1] M. Z. Hasan and C. L. Kane, Rev. Mod. Phys. **82**, 3045 (2010).
[2] N. P. Armitage, E. J. Mele, and A. Vishwanath, Rev. Mod. Phys. **90**, 015001 (2018).
[3] B. Yan and C. Felser, Annu. Rev. Condens. Matter Phys. **8**, 337 (2017).
[4] K. Manna, Y. Sun, L. Muechler, J. Kübler, and C. Felser, Nat. Rev. Mater. **3**, 244 (2018).
[5] H. Weng, X. Dai, and Z. Fang, J. Condens. Matter Phys. **28**, 303001 (2016).
[6] H. Gao, J. W. Venderbos, Y. Kim, and A. M. Rappe, Annu. Rev. Mater. **49**, 153 (2019).
[7] A. Burkov, Annu. Rev. Condens. Matter Phys. **9**, 359 (2018).
[8] M. Z. Hasan, S.-Y. Xu, I. Belopolski, and S.-M. Huang, Annu. Rev. Condens. Matter Phys. **8**, 289 (2017).
[9] M. Kang *et al.*, Nat. Mater. **19**, 163 (2020).
[10] B. Q. Lv, N. Xu, H. M. Weng, J. Z. Ma, P. Richard, X. C. Huang, L. X. Zhao, G. F. Chen, C. E. Matt, F. Bisti, V. N. Strocov, J. Mesot, Z. Fang, X. Dai, T. Qian, M. Shi, and H. Ding, Nat. Phys. **11**, 724 (2015).
[11] B. Q. Lv, H. M. Weng, B. B. Fu, X.P. Wang, H. Miao, J. Ma, P. Richard, X. C. Huang, L. X. Zhao, G. F. Chen, Z. Fang, X. Dai, T. Qian, and H. Ding, Phys. Rev. X **5**, 031013 (2015).
[12] S-M. Huang, S.-Y. Xu, I. Belopolski, C.-C. Lee, G. Chang, B. Wang, N. Alidoust, G. Bian, M. Neupane, C. Zhang, S. Jia, A. Bansil, H. Lin, and M. Z. Hasan, Nat. Commun. **6**, 7373 (2015).
[13] S.-Y. Xu, I. Belopolski, D. S. Sanchez, C. Zhang, G. Chang, C. Guo, G. Bian, Z. Yuan, H. Lu, T.-R. Chang *et al.*, Sci. Adv. **1**, e1501092 (2015).
[14] A. B. Sushkov, J. B. Hofmann, G. S. Jenkins, J. Ishikawa, S. Nakatsuji, S. Das Sarma, and H. D. Drew, Phys. Rev. B **92**, 241108(R) (2015).
[15] B. Q. Lv, S. Muff, T. Qian, Z. D. Song, S. M. Nie, N. Xu, P. Richard, C. E. Matt, N. C. Plumb, L. X. Zhao, G. F. Chen, Z. Fang, X. Dai, J. H. Dil, J. Mesot, M. Shi, H. M. Weng, and H. Ding, Phys. Rev. Lett. **115**, 217601 (2015).
[16] S. Murakami, New J. Phys. **9**, 356 (2007).
[17] S. Jia, S.-Y. Xu, and M. Z. Hasan, Nat. Mater. **15**, 1140 (2016).
[18] H. Weyl, Z. Phys. **56**, 330 (1929).
[19] X. Wan, A. M. Turner, A. Vishwanath, and S. Y. Savrasov, Phys. Rev. B **83**, 205101 (2011).
[20] D. Grassano, O. Pulci, A. M. Conte, and F. Bechstedt, Sci. Rep. **8**, 3534 (2018).
[21] J. Ruan, S.-K. Jian, H. Yao, H. Zhang, S.-C. Zhang, and D. Xing, Nat. Commun. **7**, 11136 (2016).
[22] A. A. Soluyanov, D. Gresch, Z. Wang, Q. Wu, M. Troyer, X. Dai, and B. A. Bernevig, Nature (London) **527**, 495 (2015).

[23] S. Singh, A. C. Garcia-Castro, I. Valencia-Jaime, F. Muñoz, and A. H. Romero, Phys. Rev. B **94**, 161116(R) (2016).

[24] S. Singh, Q. S. Wu, C. Yue, A. H. Romero, and A. A. Soluyanov, Phys. Rev. Material **2**, 114204 (2018).

[25] G. W. Winkler, S. Singh, and A. A. Soluyanov, Chin. Phys. B **28**, 077303 (2019).

[26] F. C. Chen, H. Y. Lv, X. Luo, W. J. Lu, Q. L. Pei, G. T. Lin, Y. Y. Han, X. B. Zhu, W. H. Song, and Y. P. Sun, Phys. Rev. B **94**, 235154 (2016).

[27] Q. L. Pei, W. J. Meng, X. Luo, H. Y. Lv, F. C. Chen, W. J. Lu, Y. Y. Han, P. Tong, W. H. Song, Y. B. Hou, Q. Y. Lu, and Y. P. Sun, Phys. Rev. B **96**, 075132(R) (2017).

[28] S. Thirupathaiah, R. Jha, B. Pal, J. S. Matias, P. K. Das, P. K. Sivakumar, I. Vobornik, N. C. Plumb, M. Shi, R. A. Ribeiro, and D. D. Sarma, Phys. Rev. B **95**, 241105 (2017).

[29] S. Lee, J. Jang, S.-I. Kim, S.-G. Jung, J. Kim, S. Cho, S. W. Kim, J. Y. Rhee, K.-S. Park, and T. Park, Sci. Rep. **8**, 13937 (2018).

[30] S.-Y. Xu, I. Belopolski, N. Alidoust, M. Neupane, G. Bian, C. Zhang, R. Sankar, G. Chang, Z. Yuan, C.-C. Lee *et al.*, Science **349**, 613 (2015).

[31] N. Xu, H. Weng, B. Lv, C. E. Matt, J. Park, F. Bisti, V. N. Strocov, D. Gawryluk, E. Pomjakushina, K. Conder *et al.*, Nat. Commun. **7**, 1 (2016).

[32] I. Belopolski, S.-Y. Xu, D. S. Sanchez, G. Chang, C. Guo, M. Neupane, H. Zheng, C.-C. Lee, S.-M. Huang, G. Bian, N. Alidoust, T.-R. Chang, B. K. Wang, X. Zhang, A. Bansil, H.-T. Jeng, H. Lin, S. Jia, and M. Z. Hasan, Phys. Rev. Lett. **116**, 066802 (2016).

[33] A. Tamai, Q. S. Wu, I. Cucchi, F. Y. Bruno, S. Riccò, T. K. Kim, M. Hoesch, C. Barreteau, E. Giannini, C. Besnard, A. A. Soluyanov, and F. Baumberger, Phys. Rev. X **6**, 031021 (2016).

[34] G. Autès, D. Gresch, M. Troyer, A. A. Soluyanov, and O. V. Yazyev, Phys. Rev. Lett. **117**, 066402 (2016).

[35] W. Zhang, Q. Wu, L. Zhang, S.-W. Cheong, A. A. Soluyanov, and W. Wu, Phys. Rev. B **96**, 165125 (2017).

[36] M. P. Ghimire, J. I. Facio, J.-S. You, L. Ye, J. G. Checkelsky, S. Fang, E. Kaxiras, M. Richter, and J. van den Brink, Phys. Rev. Research **1**, 032044(R) (2019).

[37] S. Singh, J. Kim, K. M. Rabe, and D. Vanderbilt, Phys. Rev. Lett. **125**, 046402 (2020).

[38] G. Chang, S.-Y. Xu, D. S. Sanchez, S.-M. Huang, C.-C. Lee, T.-R. Chang, G. Bian, H. Zheng, I. Belopolski, N. Alidoust *et al.*, Sci. Adv. **2**, e1600295 (2016).

[39] K. Koepernik, D. Kasinathan, D. V. Efremov, S. Khim, S. Borisenko, B. Büchner, and J. van den Brink, Phys. Rev. B **93**, 201101(R) (2016).

[40] B. Sipos, A. F. Kusmartseva, A. Akrap, H. Berger, L. Forró, and E. Tutiš, Nat. Mater. **7**, 960 (2008).

[41] X. Qian, J. Liu, L. Fu, and J. Li, Science **346**, 1344 (2014).

[42] R. Morris, R. Coleman, and R. Bhandari, Phys. Rev. B **5**, 895 (1972).

[43] H. Takahashi, T. Akiba, K. Imura, T. Shiino, K. Deguchi, N. K. Sato, H. Sakai, M. S. Bahramy, and S. Ishiwata, Phys. Rev. B **95**, 100501(R) (2017).

[44] Y. Qi, P. G. Naumov, M. N. Ali, C. R. Rajamathi, W. Schnelle, O. Barkalov, M. Hanfland, S.-C. Wu, C. Shekhar, Y. Sun *et al.*, Nat. Commun. **7**, 11038 (2016).

[45] F. C. Chen, X. Luo, J. Yan, Y. Sun, H. Y. Lv, W. J. Lu, C. Y. Xi, P. Tong, Z. G. Sheng, X. B. Zhu, W. H. Song, and Y. P. Sun, Phys. Rev. B **98**, 041114(R) (2018).

[46] F.-T. Huang, S. J. Lim, S. Singh, J. Kim, L. Zhang, J.-W. Kim, M.-W. Chu, K. M. Rabe, D. Vanderbilt, and S.-W. Cheong, Nat. Commun. **10**, 4211 (2019).

[47] C. Heikes, I.-L. Liu, T. Metz, C. Eckberg, P. Neves, Y. Wu, L. Hung, P. Piccoli, H. Cao, J. Leao, J. Paglione, T. Yildirim, N. P. Butch, and W. Ratcliff, Phys. Rev. Material **2**, 074202 (2018).

[48] H. Wei, S.-P. Chao, and V. Aji, Phys. Rev. B **89**, 014506 (2014).

[49] P. Hosur, X. Dai, Z. Fang, and X.-L. Qi, Phys. Rev. B **90**, 045130 (2014).

[50] P. Li, W. Wu, Y. Wen, C. Zhang, J. Zhang, S. Zhang, Z. Yu, S. A. Yang, A. Manchon, and X.-X. Zhang, Nat. Commun. **9**, 3990 (2018).

[51] F. Y. Bruno, A. Tamai, Q. S. Wu, I. Cucchi, C. Barreteau, A. de la Torre, S. McKeownWalker, S. Riccó, Z. Wang, T. K. Kim, M. Hoesch, M. Shi, N. C. Plumb, E. Giannini, A. A. Soluyanov, and F. Baumberger, Phys. Rev. B **94**, 121112 (2016).

[52] Y. Wu, D. Mou, N. H. Jo, K. Sun, L. Huang, S. L. Bud'ko, P. C. Canfield, and A. Kaminski, Phys. Rev. B **94**, 121113(R) (2016).

[53] P. Li, Y. Wen, X. He, Q. Zhang, C. Xia, Z.-M. Yu, S. A. Yang, Z. Zhu, H. N. Alshareef, and X.-X. Zhang, Nat. Commun. **8**, 2150 (2017).

[54] Y.-Y. Lv, X. Li, B.-B. Zhang, W. Y. Deng, S.-H. Yao, Y. B. Chen, J. Zhou, S.-T. Zhang, M.-H. Lu, L. Zhang, M. Tian, L. Sheng, and Y.-F. Chen, Phys. Rev. Lett. **118**, 096603 (2017).

[55] L. Huang, T. M. McCormick, M. Ochi, Z. Zhao, M.-T. Suzuki, R. Arita, Y. Wu, D. Mou, H. Cao, J. Yan *et al.*, Nat. Mater. **15**, 1155 (2016).

[56] K. Deng, G. Wan, P. Deng, K. Zhang, S. Ding, E. Wang, M. Yan, H. Huang, H. Zhang, Z. Xu *et al.*, Nat. Phys. **12**, 1105 (2016).

[57] M. Sakano, M. S. Bahramy, H. Tsuji, I. Araya, K. Ikeura, H. Sakai, S. Ishiwata, K. Yaji, K. Kuroda, A. Harasawa, S. Shin, and K. Ishizaka, Phys. Rev. B **95**, 121101(R) (2017).

[58] Y. Sun, S.-C. Wu, M. N. Ali, C. Felser, and B. Yan, Phys. Rev. B **92**, 161107 (2015).

[59] Z. Wang, D. Gresch, A. A. Soluyanov, W. Xie, S. Kushwaha, X. Dai, M. Troyer, R. J. Cava, and B. A. Bernevig, Phys. Rev. Lett. **117**, 056805 (2016).

[60] J. Jiang, Z. Liu, Y. Sun, H. Yang, C. Rajamathi, Y. Qi, L. Yang, C. Chen, H. Peng, C. Hwang *et al.*, Nat. Commun. **8**, 13973 (2017).

[61] A. Liang, J. Huang, S. Nie, Y. Ding, Q. Gao, C. Hu, S. He, Y. Zhang, C. Wang, B. Shen *et al.*, arXiv:1604.01706.

[62] S. Dissanayake, C. Duan, J. Yang, J. Liu, M. Matsuda, C. Yue, J. A. Schneeloch, J. C. Y. Teo, and D. Louca, npj Quantum Mater. **4**, 45 (2019).

[63] N. Aryal and E. Manousakis, Phys. Rev. B **99**, 035123 (2019).

[64] N. Xu, Z. W. Wang, A. Magrez, P. Bugnon, H. Berger, C. E. Matt, V. N. Strocov, N. C. Plumb, M. Radovic, E. Pomjakushina, K. Conder, J. H. Dil, J. Mesot, R. Yu, H. Ding, and M. Shi, Phys. Rev. Lett. **121**, 136401 (2018).

[65] Y.-Y. Lv, L. Cao, X. Li, B.-B. Zhang, K. Wang, B. Pang, L. Ma, D. Lin, S.-H. Yao, J. Zhou, Y. B. Chen, S.-T. Dong, W.

Liu, M.-H. Lu, Y. Chen, and Y.-F. Chen, Sci. Rep. **7**, 44587 (2017).
[66] X.-J. Yan, Y.-Y. Lv, L. Li, X. Li, S.-H. Yao, Y.-B. Chen, X.-P. Liu, H. Lu, M.-H. Lu, and Y.-F. Chen, Appl. Phys. Lett. **110**, 211904 (2017).
[67] S. M. Oliver, R. Beams, S. Krylyuk, I. Kalish, A. K. Singh, A. Bruma, F. Tavazza, J. Joshi, I. R. Stone, S. J. Stranick *et al.*, 2D Mater. **4**, 045008 (2017).
[68] D. Rhodes *et al.*, Nano Lett. **17**, 1616 (2017).
[69] O. B. Aslan, I. M. Datye, M. J. Mleczko, K. Sze Cheung, S. Krylyuk, A. Bruma, I. Kalish, A. V. Davydov, E. Pop, and T. F. Heinz, Nano Lett. **18**, 2485 (2018).
[70] J. A. Schneeloch, Y. Tao, C. Duan, M. Matsuda, A. A. Aczel, J. A. Fernandez-Baca, G. Xu, J. C. Neuefeind, J. Yang, and D. Louca, Phys. Rev. B **102**, 054105 (2020).
[71] V. Marchenkov, A. Domozhirova, A. Makhnev, E. Shreder, S. Naumov, V. Chistyakov, J. Huang, and M. Eisterer, Low Temp. Phys. **45**, 241 (2019).
[72] Y. Tao, J. A. Schneeloch, C. Duan, M. Matsuda, S. E. Dissanayake, A. A. Aczel, J. A. Fernandez-Baca, F. Ye, and D. Louca, Phys. Rev. B **100**, 100101(R) (2019).
[73] R. Dahal, L. Z. Deng, N. Poudel, M. Gooch, Z. Wu, H. C. Wu, H. D. Yang, C. K. Chang, and C. W. Chu, Phys. Rev. B **101**, 140505(R) (2020).
[74] I. Belopolski *et al.*, Phys. Rev. B **94**, 085127 (2016).
[75] T.-R. Chang, S.-Y. Xu, G. Chang, C.-C. Lee, S.-M. Huang, B. Wang, G. Bian, H. Zheng, D. S. Sanchez, I. Belopolski *et al.*, Nat. Commun. **7**, 1 (2016).
[76] I. Belopolski, D. S. Sanchez, Y. Ishida, X. Pan, P. Yu, S.-Y. Xu, G. Chang, T.-R. Chang, H. Zheng, N. Alidoust *et al.*, Nat. Commun. **7**, 13643 (2016).
[77] P. Li, Y. Deng, C.-H. Hsu, C. Zhu, J. Cui, X. Yang, J. Zhou, Y.-C. Hung, J. Fan, Z. Ji, F. Qu, J. Shen, C. Yang, X. Jing, H. Lin, Z. Liu, L. Lu, and G. Liu, Phys. Rev. B **104**, 085423 (2021).
[78] B. Ramshaw, K. A. Modic, A. Shekhter, Y. Zhang, E.-A. Kim, P. J. Moll, M. D. Bachmann, M. Chan, J. Betts, F. Balakirev *et al.*, Nat. Commun. **9**, 2217 (2018).
[79] E. V. Gorbar, V. A. Miransky, I. A. Shovkovy, and P. O. Sukhachov, Low Temp. Phys. **44**, 487 (2018).
[80] J. Hu, S.-Y. Xu, N. Ni, and Z. Mao, Annu. Rev. Mater. Res. **49**, 207 (2019).
[81] N. P. Ong and S. Liang, Nat. Rev. Phys. **3**, 394 (2021).
[82] I. Sodemann and L. Fu, Phys. Rev. Lett. **115**, 216806 (2015).
[83] Q. Ma *et al.*, Nature (London) **565**, 337 (2019).
[84] F. de Juan, A. G. Grushin, T. Morimoto, and J. E. Moore, Nat. Commun. **8**, 15995 (2017).
[85] E. J. König, H.-Y. Xie, D. A. Pesin, and A. Levchenko, Phys. Rev. B **96**, 075123 (2017).
[86] Y. Zhang, H. Ishizuka, J. van den Brink, C. Felser, B. Yan, and N. Nagaosa, Phys. Rev. B **97**, 241118(R) (2018).
[87] G. Liu, Nonlinear Optical Responses in Type-II Weyl Semimetals, Ph.D. Thesis, University of Pennsylvania, Philadelphia, 2019.
[88] Q. Xu, Y. Zhang, K. Koepernik, W. Shi, J. van den Brink, C. Felser, and Y. Sun, npj Comput. Mater. **6**, 32 (2020).
[89] G. Kresse and J. Furthmüller, Phys. Rev. B **54**, 11169 (1996).
[90] G. Kresse and J. Furthmüller, Comput. Mater. Sci. **6**, 15 (1996).
[91] G. Kresse and D. Joubert, Phys. Rev. B **59**, 1758 (1999).
[92] J. P. Perdew, A. Ruzsinszky, G. I. Csonka, O. A. Vydrov, G. E. Scuseria, L. A. Constantin, X. Zhou, and K. Burke, Phys. Rev. Lett. **100**, 136406 (2008).
[93] J. Klimeš, D. R. Bowler, and A. Michaelides, Phys. Rev. B **83**, 195131 (2011).
[94] T. Thonhauser, V. R. Cooper, S. Li, A. Puzder, P. Hyldgaard, and D. C. Langreth, Phys. Rev. B **76**, 125112 (2007).
[95] M. Dion, H. Rydberg, E. Schröder, D. C. Langreth, and B. I. Lundqvist, Phys. Rev. Lett. **92**, 246401 (2004).
[96] A. Togo and I. Tanaka, Scr. Mater. **108**, 1 (2015).
[97] S. Singh, L. Lang, V. Dovale-Farelo, U. Herath, P. Tavadze, F.-X. Coudert, and A. H. Romero, Comput. Phys. Commun. **267**, 108068 (2021).
[98] S. Singh, I. Valencia-Jaime, O. Pavlic, and A. H. Romero, Phys. Rev. B **97**, 054108 (2018).
[99] K. Koepernik and H. Eschrig, Phys. Rev. B **59**, 1743 (1999).
[100] U. Herath, P. Tavadze, X. He, E. Bousquet, S. Singh, F. Muñoz, and A. H. Romero, Comput. Phys. Commun. **251**, 107080 (2020).
[101] K. Momma and F. Izumi, J. Appl. Crystallogr. **44**, 1272 (2011).
[102] See Supplemental Material at http://link.aps.org/supplemental/10.1103/PhysRevB.105.125138 for detailed information about the XRD spectra, phonon spectra, Raman- and infrared-active phonon frequencies, DOS, and distribution of WPs calculated at higher pressures.
[103] P. Vinet, J. Ferrante, J. H. Rose, and J. R. Smith, J. Geophys. Res. **92**, 9319 (1987).
[104] P. Vinet, J. H. Rose, J. Ferrante, and J. R. Smith, J. Condens. Matter Phys. **1**, 1941 (1989).
[105] P. Lu, J.-S. Kim, J. Yang, H. Gao, J. Wu, D. Shao, B. Li, D. Zhou, J. Sun, D. Akinwande, D. Xing, and J.-F. Lin, Phys. Rev. B **94**, 224512 (2016).
[106] R. Dynes, Solid State Commun. **10**, 615 (1972).
[107] H. Paudyal, S. Poncé, F. Giustino, and E. R. Margine, Phys. Rev. B **101**, 214515 (2020).
[108] W. Setyawan and S. Curtarolo, Comput. Mater. Sci. **49**, 299 (2010).